The Plant Cell, Vol. 19: 549–563, February 2007, www.plantcell.org © 2007 American Society of Plant Biologists

Arabidopsis irregular xylem8 and *irregular xylem9*: Implications for the Complexity of Glucuronoxylan Biosynthesis [W]

Maria J. Peña,[a] Ruiqin Zhong,[b] Gong-Ke Zhou,[b] Elizabeth A. Richardson,[b] Malcolm A. O'Neill,[a] Alan G. Darvill,[a,c] William S. York,[a,c,1] and Zheng-Hua Ye[b,1]

[a] Complex Carbohydrate Research Center, University of Georgia, Athens, Georgia 30602
[b] Department of Plant Biology, University of Georgia, Athens, Georgia 30602
[c] Department of Biochemistry and Molecular Biology, University of Georgia, Athens, Georgia 30602

Mutations of *Arabidopsis thaliana IRREGULAR XYLEM8* (*IRX8*) and *IRX9* were previously shown to cause a collapsed xylem phenotype and decreases in xylose and cellulose in cell walls. In this study, we characterized *IRX8* and *IRX9* and performed chemical and structural analyses of glucuronoxylan (GX) from *irx8* and *irx9* plants. *IRX8* and *IRX9* are expressed specifically in cells undergoing secondary wall thickening, and their encoded proteins are targeted to the Golgi, where GX is synthesized. ^{1}H-NMR spectroscopy showed that the reducing end of *Arabidopsis* GX contains the glycosyl sequence 4-β-D-Xyl*p*-(1→4)-β-D-Xyl*p*-(1→3)-α-L-Rha*p*-(1→2)-α-D-Gal*p*A-(1→4)-D-Xyl*p*, which was previously identified in birch (*Betula verrucosa*) and spruce (*Picea abies*) GX. This indicates that the reducing end structure of GXs is evolutionarily conserved in woody and herbaceous plants. This sequence is more abundant in *irx9* GX than in the wild type, whereas *irx8* and *fragile fiber8* (*fra8*) plants are nearly devoid of it. The number of GX chains increased and the GX chain length decreased in *irx9* plants. Conversely, the number of GX chains decreased and the chain length heterodispersity increased in *irx8* and *fra8* plants. Our results suggest that IRX9 is required for normal GX elongation and indicate roles for IRX8 and FRA8 in the synthesis of the glycosyl sequence at the GX reducing end.

INTRODUCTION

Glucuronoxylans (GXs) together with cellulose and lignin are the three major components of secondary cell walls in woody plant tissues, which constitute the bulk of terrestrial biomass. The biosynthesis of cellulose and lignin has been studied intensively (Boerjan et al., 2003; Scheible and Pauly, 2004; Lerouxel et al., 2006; Somerville, 2006), whereas the mechanisms of GX biosynthesis are poorly understood. GX is composed of a linear backbone of β-(1-4)-linked D-xylosyl (Xyl) residues, some of which bear a single α-D-glucuronic acid (GlcA) or 4-*O*-methyl-α-D-glucuronic acid (MeGlcA) residue at O2 (Figure 1). The Xyl residues can also be substituted with arabinosyl and acetyl residues (Ebringerová and Heinze, 2000). Early work established that GX isolated from birch (*Betula verrucosa*) and spruce (*Picea abies*) wood contains the glycosyl sequence 4-β-D-Xyl*p*-(1→4)-β-D-Xyl*p*-(1→3)-α-L-Rha*p*-(1→2)-α-D-Gal*p*A-(1→4)-D-Xyl*p* at the reducing end (Shimizu et al., 1976; Johansson and Samuelson, 1977; Andersson et al., 1983).

Based on GX structure, it is likely that a number of glycosyltransferases (GTs) are required for the initiation, elongation, and termination of the xylan backbone, together with enzymes that add and modify side chains. Xylosyltransferase and glucuronyltransferase activities have been detected in numerous plants (Dalessandro and Northcote, 1981a, 1981b; Waldron and Brett, 1983; Baydoun et al., 1989; Suzuki et al., 1991; Porchia and Scheller, 2000; Kuroyama and Tsumuraya, 2001; Gregory et al., 2002). However, none of the genes encoding these enzymes has been identified, nor have any of the enzymes been purified to homogeneity and biochemically characterized.

Recent genomic analysis of wood formation in poplar (*Populus* species) revealed 25 putative GTs whose expression is associated with secondary wall synthesis (Aspeborg et al., 2005). *Arabidopsis thaliana* homologs of three poplar wood–associated GTs, FRAGILE FIBER8 (FRA8), IRREGULAR XYLEM8 (IRX8), and IRX9, have been shown to be required for normal vessel morphology and wall thickness and for normal amounts of xylose and cellulose in cell walls (Brown et al., 2005; Persson et al., 2005; Zhong et al., 2005). The *FRA8* gene, which encodes a putative GT in family GT47 (Coutinho et al., 2003), is specifically expressed in cells undergoing secondary wall thickening. Plants carrying mutations in this gene have reduced amounts of wall GX and a decreased ratio of GlcA to MeGlcA residues in the GX (Zhong et al., 2005). Expression of the poplar (*Populus alba* × *tremula*) *GT47C* gene in *fra8* plants rescues the defects in secondary wall thickness and GX synthesis, suggesting that GT47C is a functional homolog of FRA8 (Zhou et al., 2006).

The *IRX8* gene encodes a putative GT in family GT8 (Brown et al., 2005; Persson et al., 2005). The expression of several genes encoding GTs in family GT8 (Coutinho et al., 2003) is associated with wood formation in poplar (Aspeborg et al., 2005). Homologs of these wood-associated GTs are present in *Arabidopsis*, and several of them, including IRX8, At4g33330, At3g18660, and

[1] To whom correspondence should be addressed. E-mail will@ccrc.uga.edu or zhye@plantbio.uga.edu; fax 706-542-4412 or 706-542-1805. The authors responsible for distribution of materials integral to the findings presented in this article in accordance with the policy described in the Instructions for Authors (www.plantcell.org) are: William S. York (will@ccrc.uga.edu) and Zheng-Hua Ye (zhye@plantbio.uga.edu).
[W] Online version contains Web-only data.
www.plantcell.org/cgi/doi/10.1105/tpc.106.049320

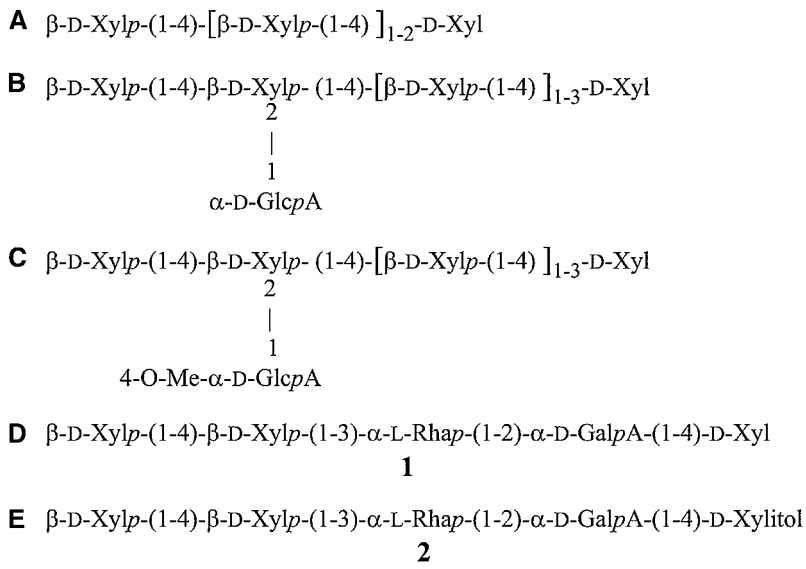

Figure 1. Structures of the Xylo-Oligosaccharides Generated by Endoxylanase Treatment of *Arabidopsis* GX.

(A) 1,4-Linked β-D-xylo-oligosaccharides.
(B) 1,4-Linked β-D-xylo-oligosaccharides partially substituted at O2 with glucuronic acid.
(C) 1,4-Linked β-D-xylo-oligosaccharides partially substituted at O2 with 4-*O*-methyl glucuronic acid.
(D) The glycosyl sequence (**1**) at the reducing end of *Arabidopsis* GXs.
(E) The glycosyl sequence (**2**) of the tetraglycosyl-xylitol.
The xylo-oligosaccharides are generated by treating the 1 and 4 N KOH–soluble materials with endoxylanase. The xylitol of glycosyl sequence **2** is formed from the reducing xylose of glycosyl sequence **1** when glucuronoxylans are solubilized from cell walls using alkali-containing $NaBH_4$. $NaBH_4$ converts the reducing xylose to xylitol. Glycosyl sequence **2** was isolated from the endoxylanase digests by reverse-phase HPLC.

At1g19300, are highly expressed in *Arabidopsis* stems (Brown et al., 2005; Persson et al., 2005; Ye et al., 2006). Several members of the GT8 family catalyze the transfer of uronic acids to glycans. For example, three *Arabidopsis* GT8 proteins, QUASIMODO1 (QUA1) (Bouton et al., 2002), PARVUS (Lao et al., 2003), and GALACTURONOSYL TRANSFERASE1 (GAUT1) (Sterling et al., 2006), have been identified and are believed to have a role in pectin biosynthesis. Of these three, only GAUT1 has been biochemically characterized and shown to have galacturonosyltransferase activity (Sterling et al., 2006).

Mutation of the *IRX9* gene, which encodes a putative GT in family GT43 (Coutinho et al., 2003), was shown to result in plants with decreased amounts of wall GX, suggesting that this gene is required for GX synthesis (Bauer et al., 2006). The poplar (*Populus tremula* × *tremuloides*) *GT43A* and Ptt *GT43B* genes, which are homologs of *IRX9*, have been shown to be highly expressed during wood formation (Aspeborg et al., 2005). In addition, a cotton (*Gossypium hirsutum*) gene, which resides in the same phylogenetic subgroup as Ptt *GT43A*, Ptt *GT43B*, and *IRX9*, is highly expressed during cotton fiber development (Wu and Liu, 2005). Together, these findings suggest that family 43 GTs have an important role in secondary wall synthesis.

In this report, we show that *IRX8* and *IRX9* are specifically expressed in fibers and vessels and that their encoded proteins are localized in the Golgi. We also show that glycosyl sequence **1** (Figure 1) is located at the reducing end of *Arabidopsis* GX. We further demonstrate that the *irx8*, *irx9*, and *fra8* mutations result in changes in the abundance of this reducing end sequence and lead to alterations in the number and length of GX chains compared with wild-type GX. Our results provide evidence for the possible involvement of IRX8 and FRA8 in the synthesis of the reducing end sequence of GXs and suggest that IRX9 has an essential role in the elongation of the xylan backbone.

RESULTS

IRX8 and *IRX9* Are Specifically Expressed in Fibers and Vessels

The interfascicular fibers of *Arabidopsis* inflorescence stems deposit a massive amount of secondary walls and provide a model system for studying the mechanisms of secondary wall synthesis (Zhong et al., 2001). During a search for xylan biosynthetic genes that are highly expressed in interfascicular fibers, we found that two GT genes, At5g54690 (*IRX8*) and At2g37090 (*IRX9*), exhibited an organ expression pattern similar to that of *FRA8*, based on expression data from the AtGenExpress project (Schmid et al., 2005; http://www.weigelworld.org/resources/microarray/AtGenExpress/) and RT-PCR analysis (data not shown). Further expression analysis showed that *IRX8* and *IRX9* were expressed in developing interfascicular fibers but not in parenchymatous pith cells (Figure 2A).

Mutation of the *IRX8* or *IRX9* gene causes a strong dwarf phenotype (Brown et al., 2005); thus, it is important to know whether these genes function specifically in secondary wall synthesis by examining when and where they are expressed

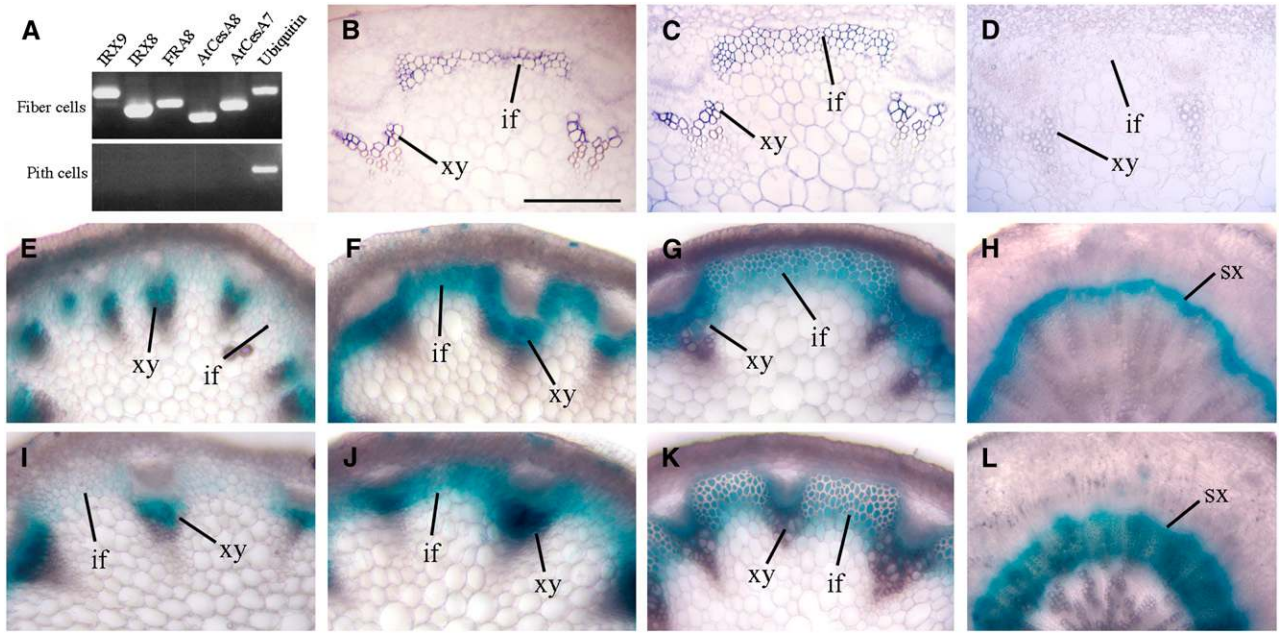

Figure 2. Expression Patterns of the *IRX8* and *IRX9* Genes in *Arabidopsis* Stems and Roots.

Cross sections of stems were hybridized with digoxigenin-labeled antisense RNA probes of *IRX8* and *IRX9*. The hybridization signals were detected using alkaline phosphatase–conjugated antibodies. Transgenic plants expressing the GUS reporter gene fused with the *IRX8* and *IRX9* genes were examined for GUS activity. if, interfascicular fiber; sx, secondary xylem; xy, xylem. Bar in **(B)** = 145 μm for **(B)** to **(L)**.

(A) RT-PCR analysis of laser-microdissected cells from stems showing the expression of *IRX8* and *IRX9* together with several other secondary wall biosynthetic genes in fiber cells but not in pith cells. The expression of a ubiquitin gene was used as an internal control.

(B) to **(D)** In situ hybridization of stem sections showing the expression of *IRX8* **(B)** and *IRX9* **(C)** genes in interfascicular fibers and developing xylem cells. A stem section hybridized with the *IRX9* sense probe is shown as a control **(D)**.

(E) to **(H)** Cross sections of stems (**[E]** to **[G]**) and roots **(H)** of transgenic *IRX8::GUS* plants showing intense GUS staining in interfascicular fibers and xylem cells undergoing secondary wall synthesis. The stem sections were from a young elongating internode **(E)**, an internode near cessation of elongation **(F)**, and a nonelongating internode **(G)**.

(I) to **(L)** Cross sections of stems (**[I]** to **[K]**) and roots **(L)** of transgenic *IRX9::GUS* plants showing strong GUS staining in interfascicular fibers and xylem cells undergoing secondary wall synthesis. The stem sections were from a young elongating internode **(I)**, an internode near cessation of elongation **(J)**, and a nonelongating internode **(K)**.

(Brown et al., 2005). To investigate their expression patterns, we fused the wild-type *IRX8* and *IRX9* genes with the β-glucuronidase (GUS) reporter gene and transformed the constructs into wild-type *Arabidopsis* plants. Analysis of GUS activity in transgenic plants revealed that *IRX8* and *IRX9* were specifically expressed in cells undergoing secondary wall thickening, including interfascicular fibers and primary and secondary xylem in stems and developing secondary xylem in roots (Figures 2E to 2L). These expression patterns were confirmed by in situ mRNA hybridization (Figures 2B to 2D). Our results demonstrate that the expression of *IRX8* and *IRX9* is specifically associated with secondary wall thickening in fibers and vessels.

IRX8 and IRX9 Are Targeted to the Golgi

The *irx8* and *irx9* mutations result in a reduction in both xylose and cellulose in cell walls (Brown et al., 2005; Bauer et al., 2006). Thus, we investigated whether the IRX8 and IRX9 proteins are located in the Golgi, where GX is synthesized, or at the plasma membrane, where cellulose is synthesized. Transgenic *Arabidopsis* plants expressing green fluorescent protein (GFP)–tagged IRX8 or IRX9 exhibited punctate fluorescence signals in the cytoplasm of root epidermal cells (Figures 3A and 3B), indicating that IRX8 and IRX9 are located in subcellular organelles. Cotransfection of yellow fluorescent protein (YFP)–tagged IRX8 or IRX9 with cyan fluorescent protein (CFP)–tagged Golgi-localized MUR4 in carrot (*Daucus carota*) protoplasts revealed their colocalization (Figures 3E to 3L), suggesting that IRX8 and IRX9 are located in the Golgi. Sequence analysis using the TMHMM2.0 program (http://www.cbs.dtu.dk/services/tmhmm-2.0/) predicted that IRX8 and IRX9 are type II membrane proteins with a single transmembrane helix at the N terminus (data not shown). These results are consistent with a role of IRX8 and IRX9 in GX biosynthesis, which is known to occur in the Golgi (Gregory et al., 2002).

irx8 Results in a Reduction in LM10 Antibody Labeling of Secondary Walls of Fibers and Vessels

The *irx8* and *irx9* mutations were shown to result in plants with abnormal vessel morphology (Brown et al., 2005; Persson et al., 2005). To extend these findings, we examined the thickness of secondary walls in two independent T-DNA insertion lines for the

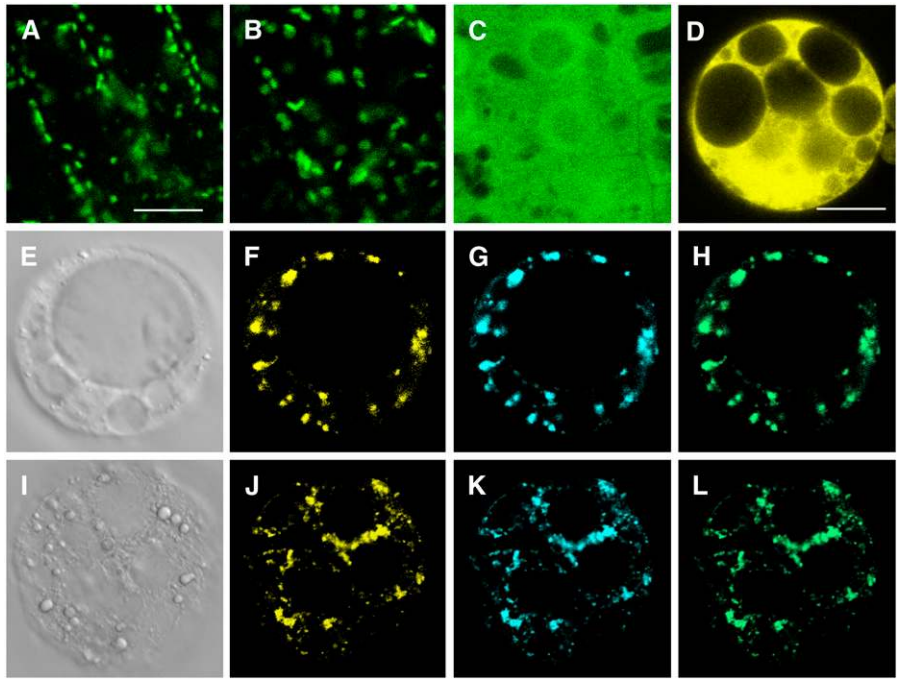

Figure 3. Subcellular Localization of Fluorescent Protein–Tagged IRX8 and IRX9 Proteins.

Fluorescent protein–tagged IRX8 and IRX9 were expressed in *Arabidopsis* plants and carrot protoplasts, and their subcellular locations were examined with a laser confocal microscope. Bar in **(A)** = 11 μm for **(A)** to **(C)**; bar in **(D)** = 21 μm for **(D)** to **(L)**.
(A) and **(B)** Confocal imaging of *Arabidopsis* root epidermal cells expressing GFP-tagged IRX8 **(A)** and GFP-tagged IRX9 **(B)** showing punctate fluorescence signals.
(C) Confocal imaging of *Arabidopsis* root epidermal cells expressing GFP alone.
(D) Confocal imaging of a carrot cell expressing YFP alone.
(E) to **(H)** Differential interference contrast image **(E)** of a carrot cell expressing IRX8-YFP and MUR4-CFP and the corresponding IRX8-YFP signals **(F)**, Golgi-localized MUR4-CFP signals **(G)**, and the merged image of IRX8-YFP and MUR4-CFP signals **(H)**.
(I) to **(L)** Differential interference contrast image **(I)** of a carrot cell expressing IRX9-YFP and MUR4-CFP and the corresponding IRX9-YFP signals **(J)**, MUR4-CFP signals **(K)**, and the merged image of IRX9-YFP and MUR4-CFP signals **(L)**.

IRX8 (*irx8-1*, SALK_008642; *irx8-2*, SALK_014026) and *IRX9* (*irx9-1*, SALK_058238; *irx9-2*, SALK_057033) genes. We found that the wall thickness of interfascicular fibers (Figures 4A to 4F) and vessels (data not shown) in the stems of *irx8* and *irx9* mutants was decreased by ~60% compared with the wild type, which is most likely the cause of their reduced stem strength (Figure 4K). In addition, the wall thickness of xylary fibers and vessels in the secondary xylem of roots was also reduced (Figures 4G to 4I). The reduced secondary wall thickness phenotype caused by mutations of the *IRX8* and *IRX9* genes is consistent with their expression patterns. The defects in secondary wall thickness, stem strength, and plant growth in both mutants were rescued by expression of their corresponding wild-type genes (Figures 4J and 4K), confirming that these phenotypes were caused directly by mutations of the *IRX8* and *IRX9* genes.

To investigate whether the *irx8* mutation affects GX deposition in secondary walls, we performed immunolocalization of GX using monoclonal antibodies LM10 and LM11. LM10 has been reported to bind to 4-*O*-methylglucuronoxylan but not to arabinoxylan and glucuronoarabinoxylan, whereas LM11 interacts with both 4-*O*-methylglucuronoxylan and arabinoxylan (McCartney et al., 2005). Only LM10 labeling is shown because similar results were observed with the LM11 antibody. Immunolabeling of stem and root sections revealed strong fluorescence signals in the walls of interfascicular fibers and xylem cells in wild-type *Arabidopsis* (Figures 5A and 5D), but only weak signals were detected in the corresponding tissues of *irx8* plants (Figures 5B and 5E). Transmission electron microscopy demonstrated that the density of immunogold labeling was reduced drastically in *irx8* compared with the wild type (Figures 5G and 5H). By contrast, the fluorescence labeling of walls in *irx9* plants remained strong (Figures 4C and 4F). However, the overall intensity was reduced, most likely as a result of the reduced wall thickness. The density of the immunogold labeling of walls in *irx9* plants (Figure 5I) and wild-type plants (Figure 5G) was comparable. Our data suggest that even though both the *irx8* and *irx9* mutations caused a nearly 60% reduction in secondary wall thickness, these mutations have different effects on GX deposition in *Arabidopsis* secondary walls.

The GX Content of Cell Walls of Inflorescence Stems Is Reduced in *irx8* and *irx9* Plants

Previous studies have shown that the *irx8* and *irx9* mutations lead to a reduction in cell wall xylose, which has led to the suggestion

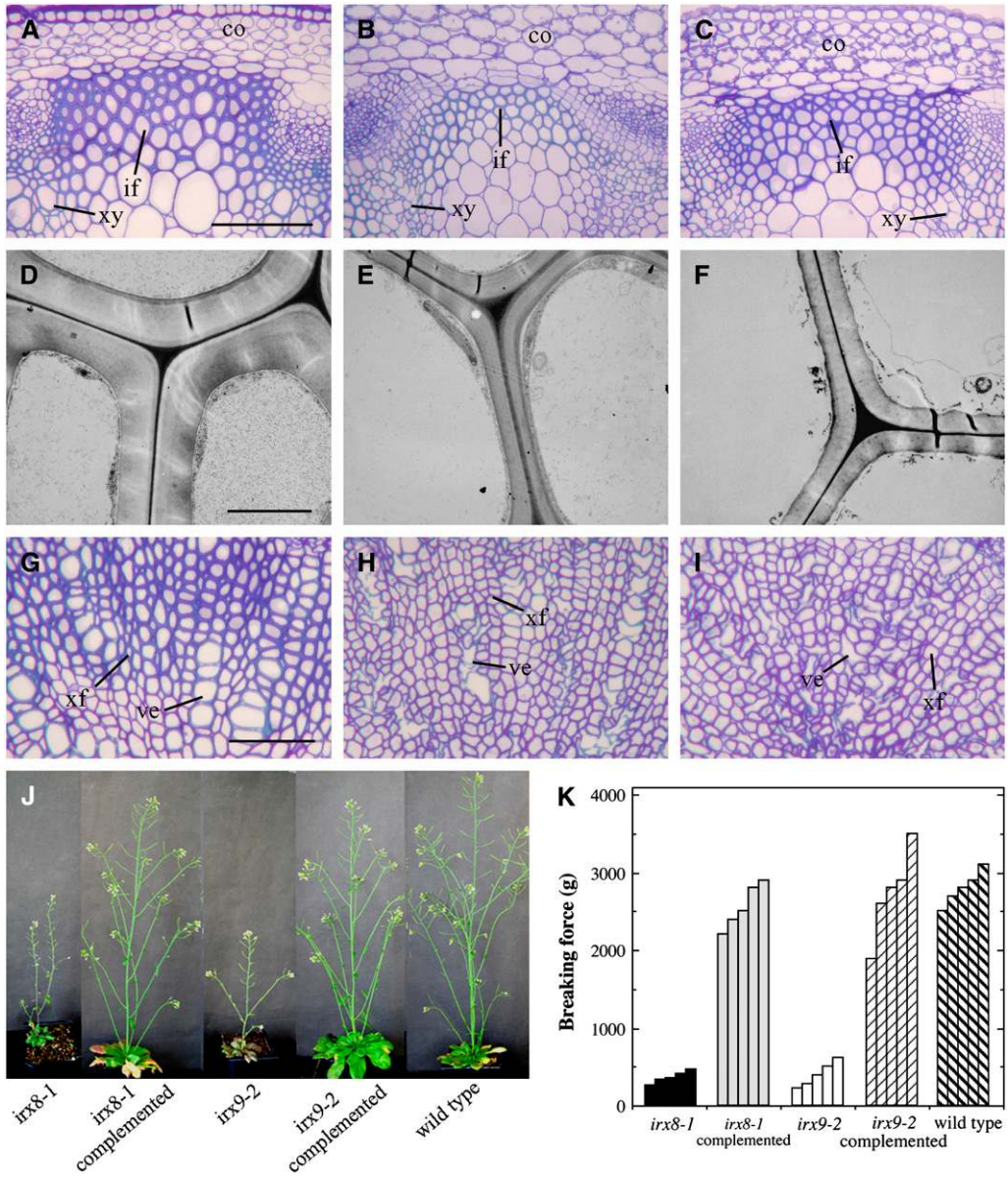

Figure 4. Reduced Secondary Wall Thickness in Fibers of *irx8* and *irx9* Plants.

Roots and bottom internodes of inflorescence stems from 10-week-old plants were sectioned for examination of fibers and vessels. co, cortex; if, interfascicular fiber; ve, vessel; xf, xylary fiber; xy, xylem. Bar in **(A)** = 120 μm for **(A)** to **(C)**; bar in **(D)** = 2.8 μm for **(D)** to **(F)**; bar in **(G)** = 67 μm for **(G)** to **(I)**.
(A) to **(C)** Cross sections of interfascicular regions of stems showing thin-walled fibers in *irx8* **(B)** and *irx9* **(C)** compared with the wild type **(A)**.
(D) to **(F)** Transmission electron micrographs of walls of interfascicular fibers in the wild type **(D)**, *irx8* **(E)**, and *irx9* **(F)**.
(G) to **(I)** Cross sections of secondary xylem regions of roots showing thin xylary fibers and deformed vessels in *irx8* **(H)** and *irx9* **(I)** compared with the wild type **(G)**.
(J) Growth defects in *irx8* and *irx9* plants were rescued by expression of the corresponding wild-type genes.
(K) Breaking force measurements showing that expression of the wild-type *IRX8* and *IRX9* genes restored the stem strength of *irx8* and *irx9*, respectively, to a level comparable with that of the wild type. Each bar represents the breaking force of the inflorescence stem of an individual plant.

that GX synthesis is affected in these mutants (Brown et al., 2005; Persson et al., 2005; Bauer et al., 2006). To confirm and extend this notion, we isolated and characterized GXs from the cell walls of inflorescence stems of wild-type, *irx8*, and *irx9* plants. We also isolated walls from *fra8* stems so that we could compare the affects on GX structure of each of the three mutations. We found that most of the xylose-rich polysaccharides are solubilized by treating the walls with 1 and 4 N KOH. At least 80% of this material remained soluble after neutralization. The *irx8*, *irx9*, and *fra8* mutations led to 57, 70, and 67% reductions, respectively, in

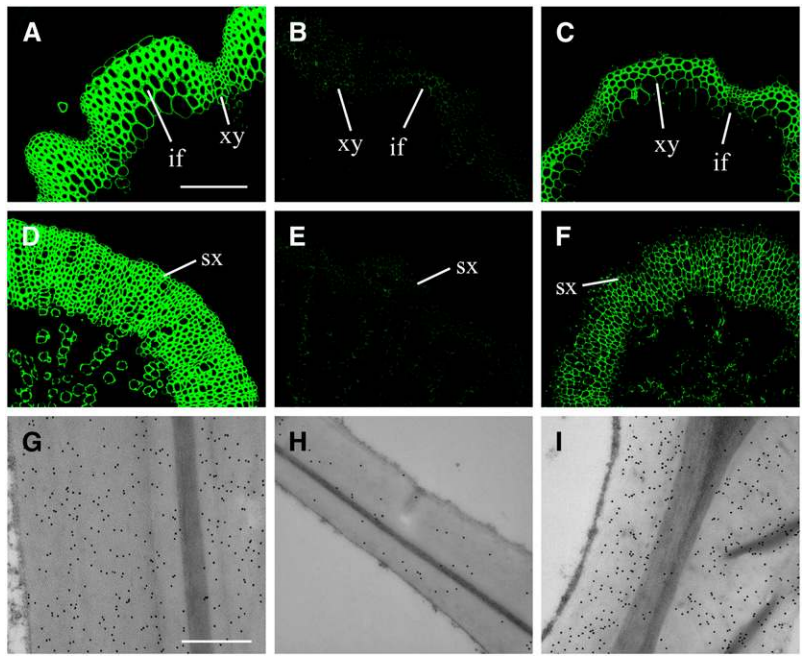

Figure 5. Immunolocalization of Xylan in the Stems and Roots of *irx8* and *irx9* Mutants.

Stem and root sections from 10-week-old *Arabidopsis* plants were used for immunolocalization of xylan with the monoclonal antibody LM10 that was generated against plant cell wall (1,4)-β-D-xylan. Xylan signals were detected with fluorescein isothiocyanate–conjugated secondary antibodies and visualized with a laser confocal microscope, or detected with gold-conjugated secondary antibodies and visualized with a transmission electron microscope. if, interfascicular fiber; sx, secondary xylem; xy, xylem. Bar in **(A)** = 154 μm for **(A)** to **(F)**; bar in **(G)** = 0.52 μm for **(G)** to **(I)**.
(A) to **(C)** Xylan immunofluorescence signals in stem sections of the wild type **(A)**, *irx8* **(B)**, and *irx9* **(C)**.
(D) to **(F)** Xylan immunofluorescence signals in root sections of the wild type **(D)**, *irx8* **(E)**, and *irx9* **(F)**.
(G) to **(I)** Immunogold labeling of xylan in fiber walls of the wild type **(G)**, *irx8* **(H)**, and *irx9* **(I)**.

the xylose content of these extracts (Table 1). We established that these changes are attributable to a decrease in GX content by showing similar reductions in the amounts of xylo-oligosaccharides that are generated by treating the KOH extracts with endoxylanase (Table 2). NMR analysis indicated that the high-molecular-weight material remaining after endoxylanase treatment contained little if any GX and that xyloglucan and pectin are the predominant polysaccharide components of this fraction. Together, these results indicate that the recovered xylo-oligosaccharides represent the majority of the KOH-solubilized GX.

irx8, *irx9*, and *fra8* Affect the Abundance of the Sequence 4-β-D-Xyl*p*-(1→4)-β-D-Xyl*p*-(1→3)-α-L-Rha*p*-(1→2)-α-D-Gal*p*A-(1→4)-D-Xyl*p* That Is Present at the Reducing End of *Arabidopsis* GX

To further investigate changes in GX structure and establish GX chemotypes for each mutant, we used size-exclusion chromatography (SEC) to separate the neutral and acidic xylo-oligosaccharides generated by endoxylanase treatment of the 1 N KOH–soluble material from wild-type, *irx8*, and *irx9* plants (data not shown). All six fractions were analyzed by matrix-assisted laser desorption/ionization time-of-flight mass spectrometry (MALDI-TOF MS). The MALDI-TOF spectra of the fractions contained $[M + Na]^+$ ions, indicating the presence of the expected products (Figures 1A to 1C): Xyl_{3-4} (*m/z* 437 and 569) in the neutral fractions and Xyl_{4-6}GlcA (*m/z* 745, 877, and 1009) and Xyl_{4-6}MeGlcA (*m/z* 759, 891, and 1023) in the acidic fractions. The ^{1}H-NMR spectra of the acidic fractions (Figure 6, Table 3) showed that in the wild type, *irx8*, and *irx9*, the GlcA:MeGlcA ratios were 0.76, 0.06, and 0.03, respectively. A similar decrease in the proportion of GlcA was observed in *fra8* GX (Zhong et al., 2005), suggesting that all three mutations lead to an alteration in GX structure.

The ^{1}H-NMR spectrum of the *irx9* acidic xylo-oligosaccharides contained several unexpected signals that were much stronger than in the wild-type spectrum and that were nearly absent in the *irx8* and *fra8* spectra (Figures 6A to 6D). To investigate the origin of these signals, we separated the acidic oligosaccharides by reverse-phase HPLC. MALDI-TOF MS of one of the fractions was enriched in an ion at *m/z* 761, consistent with the presence of an oligoglycosyl alditol. Such alditols are generated when the residue at the reducing end of the polysaccharide reacts with $NaBH_4$, which is added to the alkaline extraction medium to avoid degradation by base-catalyzed peeling reactions (Johansson and Samuelson, 1977). To improve the separation of the xylo-oligosaccharides by reverse-phase HPLC, the reducing oligosaccharides were converted to their 2-aminobenzamide derivatives. This resulted in the separation of the oligosaccharide alditol (*m/z* 761), which binds weakly to the column, from the

Table 1. Glycosyl Residue Compositions of the 1 and 4 N KOH–Soluble Materials from Wild-Type and Mutant *Arabidopsis* Stems

Cell Wall Fraction	Rha	Fucose	Ara	Xyl	Man	Gal	Glc
1 N KOH–soluble							
Wild type	2	<1	2	66	1	3	5
fra8	1	1	2	13	3	4	10
irx8	1	1	4	12	2	6	10
irx9	2	<1	3	31	2	4	12
4 N KOH–soluble							
Wild type	1	1	2	26	3	5	8
fra8	1	1	2	17	7	4	11
irx8	1	1	3	16	7	6	12
irx9	1	1	3	9	6	6	10

Data shown are means (mg sugar/g AIRs) of two duplications of two independent analyses. AIRs were treated sequentially with endopolygalacturonase and pectin methyl esterase, xyloglucan-specific endoglucanse, and 1 and 4 N KOH. The 1 and 4 N KOH–soluble materials were hydrolyzed with trifluoroacetic acid, and the released monosaccharides were converted to their alditol acetate derivatives. Gas chromatography–mass spectrometry was used for the identification and quantitation of the monosaccharides. The variance is not shown but was <10%.

2-aminobenzamide derivatives, which bind strongly. The ^{1}H-NMR spectrum of the purified oligoglycosyl alditol was dominated by the unexpected signals initially detected in the spectrum of the acidic xylo-oligosaccharide fraction from *irx9*. These signals were assigned to protons of α-Gal*p*A, α-Rha*p*, and β-Xyl*p* residues (Figure 6E, Table 4) on the basis of their scalar coupling patterns and chemical shifts in the gCOSY and TOCSY spectra. The linkages between each glycosyl residue were deduced from the interglycosidic scalar couplings observed in the high-resolution gCOSY spectrum (Jia et al., 2005) and from the interglycosidic dipolar couplings observed in NOESY and ROESY spectra (Table 4). Together, the NMR and MALDI-TOF MS analyses provide sufficient evidence to unambiguously assign the linkage and sequence of residues in the oligoglycosyl alditol as β-D-Xyl*p*-(1→4)-β-D-Xyl*p*-(1→3)-α-L-Rha*p*-(1→2)-α-D-Gal*p*A-(1→4)-D-xylitol (sequence **2**; Figure 1E). Previous studies have shown that β-D-Xyl*p*-(1→4)-β-D-Xyl*p*-(1→3)-α-L-Rha*p*-(1→2)-α-D-Gal*p*A-(1→4)-D-Xyl (sequence **1**; Figure 1D) is present at the reducing end of birch and spruce GXs (Shimizu et al., 1976; Johansson and Samuelson, 1977; Andersson et al., 1983). The reducing xylose is converted to xylitol when the GX is solubilized with KOH containing $NaBH_4$. This led us to believe that glycosyl sequence **1** is present at the reducing end of *Arabidopsis* GX and that the accumulation of this glycosyl sequence is affected in *irx8*, *irx9*, and *fra8* plants.

To confirm that glycosyl sequence **1** is indeed present at the reducing end of *Arabidopsis* GX, we solubilized GXs from *irx9* cell walls in the absence and presence of $NaBH_4$. The ^{1}H-NMR spectra of both GXs contained resonances of the internal α-Gal*p*A, α-Rha*p*, and β-Xyl*p* residues of glycosyl sequence **1** (Figures 7A and 7B). Signals for H-1 of the α and β forms of the reducing xylose were present only in the GX extracted in the absence of $NaBH_4$. The presence of this reducing sugar resulted in discernible chemical shift and anomerization effects (Sakaguchi et al., 2001) on several of the resonances of the α-Gal*p*A, α-Rha*p*, and 3-linked β-Xyl*p* residues (Figure 7A). In particular, H-5 of the α-D-Gal*p*A was split into two fully resolved signals (a and b in Figure 7A) whose intensities are comparable to those of the H-1 signals of the α and β forms of the reducing xylose (α and β in Figure 7A). This analysis verified that the 3-linked β-Xyl*p*, α-Rha*p*, and α-Gal*p*A residues are in close proximity to the xylose at the reducing end of the GX. We conclude that glycosyl sequence **1** is located at the reducing ends of GXs synthesized by *Arabidopsis* and that the abundance of this sequence is altered in *irx8*, *irx9*, and *fra8* GXs.

The Molecular Weight Distribution of GX Is Altered in *irx8*, *irx9*, and *fra8* Plants

Our data have clearly shown that the *irx8*, *irx9*, and *fra8* mutations lead to a discernible reduction in the amounts of cell wall GX and to alterations in GX structure. We then decided to determine whether the size distribution of the GX was also affected by these mutations. Toward this goal, we analyzed the 1 and 4 N KOH–soluble materials by SEC. These SEC profiles correspond to the sum of the profiles of all of the components present in the extract. Selectively removing one component and then subtracting the resulting SEC profile from the total allows a profile corresponding to that of the component that was removed to be obtained. Thus, we treated the alkali extracts with a homogenous endoxylanase and analyzed the products by SEC. The profile of the endoxylanase-treated material was then subtracted from the untreated profile (Figure 8). The resulting profile represents the material that is susceptible to endoxylanase and thus corresponds to the size distribution of the GX. We found an increase in the heterodispersity of the GXs isolated from *irx8* (Figures 8A and 8B) and *fra8* (Figures 8C and 8D) plants. Moreover, some of the GXs from these plants have a higher molecular weight than do wild-type GX (Figures 8G and 8H). By contrast, the *irx9* mutation resulted in a decrease in the molecular weight of the GX (Figures 8E and 8F). This decrease in molecular weight may account for the fact that ~90% of the *irx9* GX was solubilized by 1 N KOH, whereas the same treatment solubilized only 65% of the GX in wild-type plants (Table 2).

The Increased Size Heterogeneity of *irx8* and *fra8* GX Is Correlated with a Decrease in the Proportion of GX Molecules with Glycosyl Sequence 1 at Their Reducing Ends

Our data had provided evidence that wild-type, *irx8*, *irx9*, and *fra8* plants synthesize GXs with different size distributions (Figure

Table 2. Amounts of Wild-Type and Mutant *Arabidopsis* GXs

Plant	1 N KOH (mg/g AIRs)	4 N KOH (mg/g AIRs)	Ratio 1 N:4 N	Total (mg/g AIRs)
Wild type	81	43	1.9	124
fra8	27	25	1.1	52
irx8	18	13	1.4	31
irx9	52	4	13.0	56

The GX contents of the alkali-soluble fractions were obtained by treating the fractions with endoxylanase and measuring the amounts of xylo-oligosaccharide formed by size-exclusion chromatography with refractive index detection.

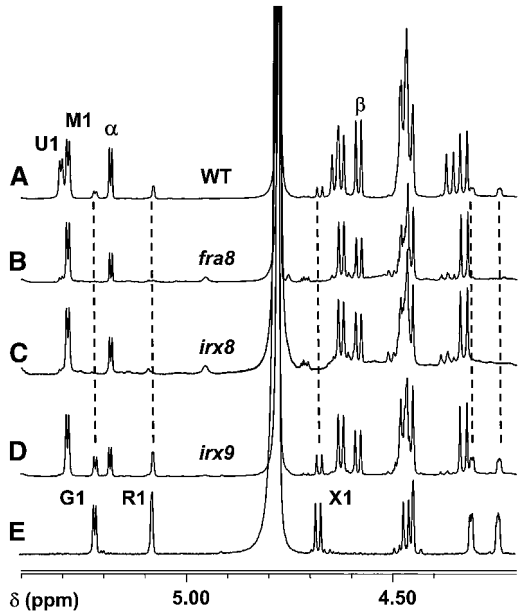

Figure 6. Anomeric Region of the 600-MHz ^{1}H-NMR Spectra of the Xylo-Oligosaccharides Generated by Endoxylanase Treatment of the Material Solubilized by 1 N KOH–Containing $NaBH_4$.

(A) Wild-type xylo-oligosaccharides.
(B) *fra8* xylo-oligosaccharides.
(C) *irx8* xylo-oligosaccharides.
(D) *irx9* xylo-oligosaccharides.
(E) Tetraglycosyl-xylitol (glycosyl sequence **2**; see Figure 1) isolated from the products generated by endoxylanase treatment of *irx9* GX.
The anomeric region shown contains diagnostic well-resolved signals for each residue in the complex. These include the following: U1, α-D-Glc*p*A H1; M1, 4-*O*-methyl α-D-Glc*p*A H1; G1, α-D-Gal*p*A H1; R1, α-L-Rha*p* H1; X1, 3-linked β-D-Xyl*p* H1; G4, α-D-Gal*p*A H4; R2, α-L-Rha*p* H2. α and β indicate the anomeric signals of α and β reducing xylose H1, respectively.

8). We initially assumed that all GX molecules solubilized by alkali-containing $NaBH_4$ would contain glycosyl sequence **2** (Figure 1E) at their reducing ends. An estimate of the average degree of polymerization of these GXs could then be obtained by integrating selected resonances of reducing oligosaccharides and glycosyl sequence **2** in the NMR spectra of the endoxylanase-generated xylo-oligosaccharides. However, during this analysis, we discovered that some of these oligomers had Xyl*p*, rather than Gal*p*A, attached to xylitol (Table 5). Our data suggest that at least 80% of the GXs from *irx8* and *fra8* plants had 4-β-D-Xyl*p*-(1→4)-D-Xyl*p* at their reducing ends (Table 6). By contrast, 98% of the GXs from *irx9* plants and 84% of wild-type GXs contain glycosyl sequence **1** at their reducing ends (Table 6). Thus, the increased size heterogeneity of *irx8* and *fra8* GXs is correlated with a decrease in the proportion of GX molecules that have glycosyl sequence **1** at their reducing ends. Furthermore, the *fra8* and *irx8* mutations result in a decrease in the number of GX molecules synthesized, whereas the primary effect of the *irx9* mutation is a decrease in the GX molecular weight (Figure 8, Table 6).

DISCUSSION

The data we have obtained in this study provide compelling evidence that glycosyl sequence **1** is present at the reducing end of *Arabidopsis* GX. This structure was first identified as a component of birch and spruce GXs (Shimizu et al., 1976; Johansson and Samuelson, 1977; Andersson et al., 1983). Our study sheds light on its biological significance.

IRX8 and FRA8 Are Required for the Synthesis of Glycosyl Sequence 1 at the Reducing End of *Arabidopsis* GX and a Normal Amount of GX Chains

Our results indicate that functional *FRA8* and *IRX8* genes (or homologous genes) are necessary for the biosynthesis of glycosyl sequence **1**, which is located at the reducing end of the GX. The presence of small amounts of this structure in these mutants may be attributable to the expression of homologs of these genes. This is in agreement with our recent finding that overexpression of a *FRA8* homolog (At5g22940) that is normally expressed at low levels in *Arabidopsis* stems can functionally complement the *fra8* mutation (our unpublished data).

We have shown that the *irx8* mutation leads to a reduction in the number of GX chains and that most of the small amount of GX that is synthesized by these plants lacks glycosyl sequence **1** at its reducing end. These findings indicate that IRX8 is involved

Table 3. ^{1}H-NMR Assignments of the Acidic Xylo-Oligosaccharides Generated by Endoxylanase Treatment of the 1 and 4 N KOH–Soluble Materials

Residue	H1	H2	H3	H4	H5	$H5_{ax}$
α-Xyl*p* (reducing)	5.183	3.543	3.807			
β-Xyl*p* (reducing)	4.583	3.249	3.546	3.779	4.055	3.377
β-Xyl*p* (internal)	4.474	3.278	3.573	3.787	4.146	3.436
β-Xyl*p* (internal)	4.478	3.297	3.548	3.791	4.108	3.373
β-Xyl*p* (terminal)	4.459	3.256	3.425	3.621	3.971	3.299
β-Xyl*p* (4Me-α-GlcA)	4.624	3.438	3.618	3.803	4.103	3.381
β-Xyl*p* (α-GlcA)	4.637	3.482	3.633	3.808	4.110	3.392
4-*O*-Methyl-α-Glc*p*A	5.285	3.572	3.758	3.218	4.327	
α-Glc*p*A	5.302	3.551	3.739	3.472	4.360	

Chemical shifts are reported in ppm relative to internal acetone, δ 2.225. β-Xyl (4Me-α-GlcA) is a β-linked xylosyl residue that is substituted at O2 with 4-*O*-methyl GlcA (see Figure 1 for details). β-Xyl (α-GlcA) is a β-linked xylosyl residue that is substituted at O2 with GlcA (see Figure 1 for details). H4 and H5 of the reducing α xylose were not assigned.

Table 4. ^{1}H-NMR Assignments of Glycosyl Sequence **2**

Residue	H1	H2	H3	H4	H5	$H5_{ax}$	H6
β-Xyl*p* (terminal)	4.464 (7.9)	3.260	3.431	3.628	3.973	3.313	
β-Xyl*p* (internal)	4.678 (7.9)	3.392	3.584	3.790	4.088	3.407	
α-Rha*p*	5.080 (1.5)	4.241	3.946	3.622	3.796		1.332
α-Gal*p*A	5.219 (3.8)	3.959	4.103	4.306	4.448		
Interglycosidic cross-peaks							
H1 β-Xyl*p* to H4 β-Xyl*p*			4.464	3.790	ROESY		
H1 β-Xyl*p* to H3 α-Rha*p*			4.678	3.946	ROESY, NOESY, and gCOSY		
H1 α-Rha*p* to H2 α-Gal*p*A			5.08	3.959	ROESY, NOESY, and gCOSY		
H1 α-Gal*p*A to xylitol			5.219	3.870	ROESY		

Chemical shifts are reported in ppm relative to internal acetone, δ 2.225. Scalar coupling constants are given in parentheses. Interglycosidic cross-peaks allow the linkage between two glycosyl residues to be determined and were obtained from the high-resolution gCOSY, ROESY, and NOESY NMR spectra.

in the synthesis of glycosyl sequence **1**, whose presence is correlated with normal GX biosynthesis. *IRX8* encodes a putative GT in family GT8 (Brown et al., 2005; Persson et al., 2005) with homology with GUAT1, an α-GalA transferase (Sterling et al., 2006), and QUA1, a putative α-GalA transferase (Bouton et al., 2002), whose expression is correlated with xylan and homogalacturonan biosynthesis (Orfila et al., 2005). Family GT8 enzymes are retaining glycosyl transferases that catalyze the formation of α-glycosidic bonds when using α-linked donor substrates such as UDP-α-D-GalA. Thus, it is possible that IRX8 catalyzes the addition of an α-D-GalA residue to *O*4 of the reducing Xyl residue of glycosyl sequence **1**.

FRA8 was shown previously to be required for the synthesis of normal amounts of GX (Zhong et al., 2005). The *FRA8* gene encodes a putative GT in family GT47 (Zhong et al., 2005). This family includes enzymes with an inverting mechanism, which usually leads to β-glycosidic linkages (when typical α-linked donor substrates are used). Thus, it is possible that FRA8 catalyzes the formation of the β-linkage of xylose to either *O*3 of the rhamnose or *O*4 of the penultimate xylose of glycosyl sequence **1** (Figure 1) if UDP-α-D-Xyl is the donor substrate. However, in plants, the addition of α-Rha residues is catalyzed by inverting GTs that use UDP-β-L-Rha as the donor substrate (Watt et al., 2004). Therefore, it is also possible that FRA8 catalyzes the addition of rhamnose during the biosynthesis of glycosyl sequence **1**.

The ratio of GlcA to MeGlcA in GXs from *irx8*, *irx9*, and *fra8* plants is lower than in wild-type GX, such that MeGlcA predominates in the mutant plants. We previously described several mechanisms that are consistent with this observation (Zhong et al., 2005). Among these was the idea that the proportion of GlcA residues methylated depends on a balance between the rate of GX synthesis and the rate at which GlcA side chains of the nascent GX are methylated (Kauss and Hassid, 1967). In this scenario, the GlcA methylation rate, which is likely to be controlled by the availability of the methyltransferase and donor substrate (*S*-adenosyl-L-Met) (Kauss and Hassid, 1967), is lower than the rate at which GlcA side chains are added. Thus, in wild-type plants, only a portion of the GlcA side chains are methylated. Conversely, methylation may keep pace with GX synthesis if the rate of GX synthesis is decreased, thereby decreasing the rate at which GlcA side chains become available as acceptor substrates. Thus, in mutant plants that produce less GX, a higher proportion of GlcA is methylated. The observation of this effect in all three mutant plants described here is consistent with this saturation mechanism.

IRX9 Is Essential for the Normal Elongation of GX Chains

The elongation of the GX chain appears to require the cooperation of the transferases that catalyze the addition of xylose to the main chain and the addition of GlcA as a side chain (Baydoun et al., 1989). Thus, our observation that *irx9* plants synthesize GX with reduced chain length could result from the disruption of either of these two processes. Our data indicate that IRX9 is not involved in the synthesis of glycosyl sequence **1** (Table 6). IRX9 is a putative GT in family GT43. Enzymes in this family are distinguished by an inverting mechanism, typically catalyzing the formation of β-glycosidic bonds using α-linked glycosyl donors. Our demonstration that the *irx9* mutation leads to a decrease in the chain length of GX suggests that *IRX9* encodes a xylan synthase responsible for adding β-xylosyl residues to the nascent GX. This hypothesis is consistent with our results indicating that *IRX9* is highly expressed in cells undergoing secondary wall biogenesis and that IRX9 is localized in the Golgi, where GX synthesis occurs (Baydoun and Brett, 1997; Gregory et al., 2002). However, it is also possible, as we discussed previously (Zhong et al., 2005), that an inverting GT can catalyze the formation of an α-linkage when a β-linked substrate (such as glycosyl phospholipids) is used as the donor. Such inverting enzymes can also catalyze the formation of high-energy β-linked glycosides (such as glycosyl phospholipids) that are subsequently used as glycosyl donors. Thus, an alternative interpretation is that IRX9 is directly or indirectly involved in the transfer of α-linked GlcA residues to the GX backbone. Additional studies are required to determine whether IRX9 catalyzes the addition of xylose or GlcA to the GX backbone.

Glycosyl Sequence 1 May Function as a Link to Other Wall Polymers

There is evidence suggesting that nascent GX is covalently attached to protein (Crosthwaite et al., 1994). We obtained no

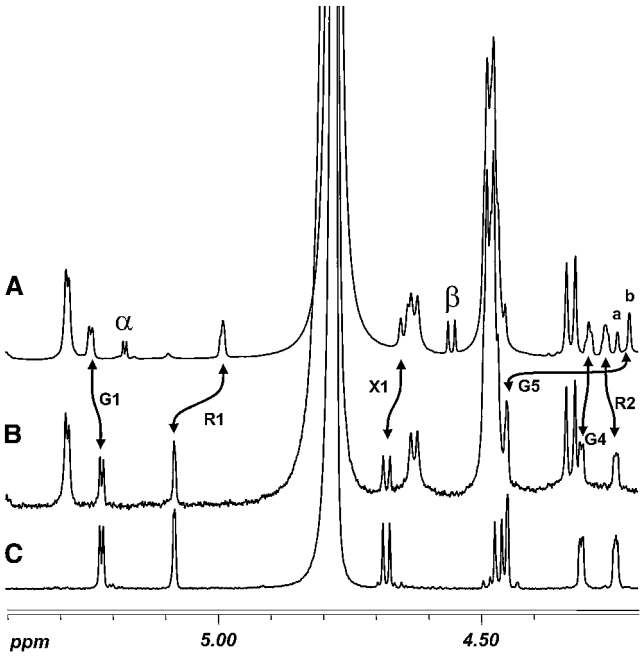

Figure 7. Anomeric Region of the 600-MHz ^{1}H-NMR Spectra of Alkali-Soluble GX from the Stems of *irx9* Plants.

(A) ^{1}H-NMR spectrum of GX extracted from *irx9* cell walls with 0.25 N KOH in the absence of $NaBH_4$.
(B) ^{1}H-NMR spectrum of GX extracted from *irx9* cell walls with 1.0 N KOH in the presence $NaBH_4$.
(C) ^{1}H-NMR spectrum of the purified glycosyl sequence **2** (see Figure 1). H1 resonances of reducing xylose residues are labeled with the anomeric configuration (α or β) of the residue. Changes in the positions of the resonance of specific nonreducing residues are indicated by double-headed arrows. G1, α-D-Gal*p*A H1; R1, α-L-Rha*p* H1; X1, 3-linked β-D-Xyl*p* H1; G5, α-D-Gal*p*A H5; G4, α-D-Gal*p*A H4; R2, α-L-Rha*p* H2. All of these resonances exhibit distinct anomerization effects in the spectrum of the GX solubilized without $NaBH_4$, especially α-D-Gal*p*A H5, which is split into two fully resolved signals labeled a and b, corresponding to the α and β forms, respectively, of the reducing xylose residue.

evidence that GX is attached to protein, or any other cell wall polymer, via glycosyl sequence **1**. If such a link exists, it is cleaved by alkali during GX extraction. Clearly, demonstration that glycosyl sequence **1** constitutes a covalent connection between GX and other wall polymers will require structural characterization of the intact link.

Models of GX Biosynthesis during Secondary Wall Formation

Our data, together with the results of previous studies (Shimizu et al., 1976; Andersson et al., 1983), show that glycosyl sequence **1** is located at the reducing ends of GXs in angiosperms and gymnosperms, suggesting that evolutionarily diverse plants synthesize GX in a similar manner. Two possible biosynthetic mechanisms that differ in the direction of xylan chain elongation and the function of glycosyl sequence **1** are consistent with our experimental observations. The first mechanism requires that glycosyl sequence **1** is a primer for GX synthesis and that the backbone is extended by adding xylose to the nonreducing end. There is precedent for this mechanism, as animal glycosaminoglycans are formed by adding monosaccharides to the nonreducing end of a linker oligosaccharide that is attached to protein via a xylose residue at the reducing end (Prydz and Dalen, 2000; Sugahara and Kitagawa, 2002). If this mechanism occurs in plants, different enzymes are likely to initiate primer synthesis, as BLAST searches of the *Arabidopsis* genomic database revealed no close homologs of the xylosyltransferase (EC 2.4.2.26) that attaches the xylosyl residue of the linker oligosaccharide in glycosaminoglycans to protein (Prydz and Dalen, 2000; Sugahara and Kitagawa, 2002). The second mechanism requires that GX is synthesized by adding monosaccharides to the reducing end

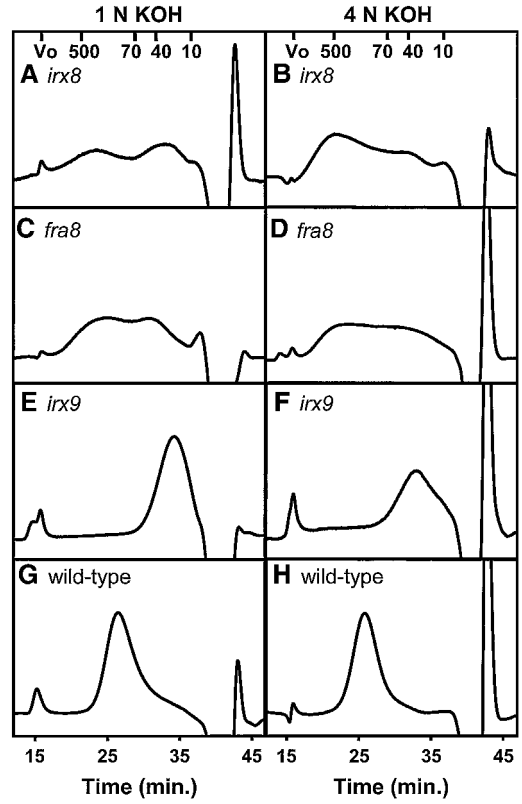

Figure 8. SEC Profiles Showing the Size Distribution of GX from *irx8*, *irx9*, *fra8*, and Wild-Type Plants.

The 1 and 4 N KOH–soluble materials from wild-type and mutant plants were treated separately with endoxylanase and analyzed by SEC. Each SEC profile was then subtracted from its corresponding SEC profile of the untreated material. This resulting profile corresponds to the size distribution profile of the GX.
(A) and **(B)** The reconstructed profiles of *irx8* GX.
(C) and **(D)** The reconstructed profiles of *fra8* GX.
(E) and **(F)** The reconstructed profiles of *irx9* GX.
(G) and **(H)** The reconstructed profiles of wild-type GX.
(A), **(C)**, **(E)**, and **(G)** show data for the 1 N KOH–soluble materials. **(B)**, **(D)**, **(F)**, and **(H)** show data for the 4 N KOH–soluble materials. The column excluded volume (Vo) and the elution positions of dextran molecular mass markers of 500, 70, 40, and 10 kD are shown.

Table 5. ^{1}H-NMR Assignments of the Xyl*p* Residues Linked to Xylitol in Oligoglycosyl-Xylitols Containing Xyl, GlcA, or 4-*O*-Methyl-GlcA

	β-Xylosyl Residues Linked to Xylitol					
Oligosaccharide	H1	H2	H3	H4	H5	$H5_{ax}$
Xyl_2-xylitol	4.580	3.352	3.574	3.782	4.101	3.379
Xyl-xylitol	4.554	3.32	3.447	3.622	3.968	3.310
(Me)GlcA-Xyl_4-xylitol	4.573	3.34	3.595	3.793	4.104	3.379
(Me)GlcAXyl_3-xylitol	4.578	3.357	3.573	3.787	4.104	3.379

These oligosaccharides were generated by $NaBH_4$ reduction of the products generated by endoxylanase treatment of wild-type GX. Chemical shifts are reported in ppm relative to internal acetone, δ 2.225.

and that transfer of glycosyl sequence **1** (either one residue at a time or en bloc) to the reducing end terminates chain elongation. The synthesis of hyaluronan (Bodevin-Authelet et al., 2005; Tlapak-Simmons et al., 2005) and starch (Mukerjea and Robyt, 2005), which have been reported to occur by the addition of monosaccharides to the reducing end, serve as precedents for this mechanism. Furthermore, the presence of GX chains that do not have glycosyl sequence **1** at the reducing end suggests either that glycosyl sequence **1** is cleaved from some of the GX chains during wall biogenesis or that GX chains can be synthesized without involving glycosyl sequence **1** as a primer. The correlation of decreased synthesis of glycosyl sequence **1** with a lower proportion of GX molecules having this structure at their reducing end supports a model in which glycosyl sequence **1** acts as a chain terminator. However, chain termination may still occur at relatively low frequency in the absence of glycosyl sequence **1** (e.g., by transfer of the nascent GX chain to water). Regardless of the actual mechanism operating in vivo, obtaining unambiguous evidence for the direction of xylan backbone elongation will be technically challenging, although a general approach to address this question has been proposed (Mukerjea and Robyt, 2005).

Several explicit models that include specific roles for the *IRX8*, *IRX9*, and *FRA8* gene products in GX biosynthesis are consistent with the available data. A common characteristic of many of these models is the requirement for multiple-subunit enzyme complexes. If this notion is correct, then it is unlikely that biochemical activity can be shown using in vitro assays based on individual gene products. The apparent complexity of the process and the products formed suggests that simple oligosaccharides may not function as acceptor substrates. Nevertheless, we expressed the recombinant IRX9 protein in yeast and assayed for xylosyltransferase activity as described (Zhong et al., 2005). However, we did not detect transferase activity (data not shown). This may be attributable to improper folding or incorrect posttranslational modification of the protein in a heterologous expression system or to the use of inappropriate acceptor substrates. In any case, our observations provide a framework for the rational design of experiments to understand GX synthesis and to assign biochemical functions to specific gene products involved in this process.

In summary, our data suggest that the coordinated action of FRA8, IRX8, and IRX9 is necessary for the regulation of GX chain length and for the normal assembly and morphology of secondary cell walls in *Arabidopsis*. FRA8 and IRX8 (or their homologs) are likely to be required for the synthesis of glycosyl sequence **1** at the reducing end of the GX, whereas IRX9 is involved in elongation of the GX chain. Our results indicate that mutating *IRX8*, *IRX9*, or *FRA8* affects the amount and extractability of GX. Understanding the functions of the proteins encoded by these genes will facilitate the targeted modification of secondary cell walls by genetic manipulation of GX biosynthesis. Using these techniques to modify the physical properties of GX will almost certainly lead to the more efficient use of plant secondary walls in energy production, wood and paper production, and nutrition.

METHODS

Plant Growth

The T-DNA insertion lines SALK_008642, SALK_014026, SALK_058238, and SALK_057033 were obtained from the ABRC. Both wild-type *Arabidopsis thaliana* (ecotype Columbia) and mutant plants were grown in a greenhouse under the same conditions.

Expression Analysis

Interfascicular fiber cells and pith cells from inflorescence stems of 5-week-old *Arabidopsis* plants were isolated using the PALM microlaser system (PALM Microlaser Technologies), and the microdissected cells were used for RNA isolation and amplification as described (Zhong et al., 2006). The amplified RNA was used in RT-PCR analysis of the expression levels of genes. PCR was performed for various numbers of cycles to determine the logarithmic phase of amplifications. The experiments were repeated three times, and identical results were obtained. RNA without reverse transcription was used as a negative control for PCR amplification, and no PCR product was detected. The expression of a ubiquitin gene was used as an internal control.

Complementation of Mutants and GUS Reporter Gene Analysis in *Arabidopsis*

A 6.4-kb genomic DNA fragment containing the *IRX8* gene (including a 2.7-kb 5′ upstream region, the entire exon and intron sequence, and a 1.4-kb 3′ downstream region) and a 6.8-kb DNA fragment containing the

Table 6. Selected Properties of Wild-Type and Mutant *Arabidopsis* GXs

	GX		
Plant	Average DP	Percentage with Glycosyl Sequence **1** at End	μmol/g AIRs
Wild type	93	84	10
fra8	80	22	5
irx8	125	4	2
irx9	28	98	14

The degree of polymerization (DP) of the GXs and the percentage of GX with glycosyl sequence **1** at the reducing end were determined from the ratios of total residues to Xyl-xylitol and GalA-xylitol estimated by ^{1}H-NMR spectroscopy. The average DP allows the molecular weight of the GX to be estimated. Dividing the amount of GX (mg/g AIRs; see Table 2) by its molecular weight allows the amount of GX (μmol/g AIRs) to be calculated (see text for details).

IRX9 gene (including a 3-kb 5′ upstream region, the entire exon and intron sequence, and a 1.5-kb 3′ downstream region) were amplified by PCR using a high-fidelity DNA polymerase with gene-specific primers and cloned into the binary vector pGPTV-HPT (Becker et al., 1992). The constructs were introduced into *irx8-1* or *irx9-2* plants, respectively, by *Agrobacterium tumefaciens*–mediated transformation (Bechtold and Bouchez, 1994). Transgenic plants were selected by growth on nutrient agar containing hygromycin and used for analysis.

The cell type and developmental expression patterns of the *IRX8* and *IRX9* genes were examined using the GUS reporter gene. The genomic DNA fragments that complemented the mutant phenotypes were used for GUS reporter gene analysis. The *GUS* gene was inserted in-frame right before the stop codon of the *IRX8* or *IRX9* gene and then cloned into the binary vector pBI101 to create the *IRX9::GUS* and *IRX8::GUS* constructs. The constructs were transformed into wild-type *Arabidopsis* for the generation of transgenic plants, which were used for expression analysis of the GUS reporter gene (Zhong et al., 2005).

In Situ Localization of mRNAs

Wild-type *Arabidopsis* stems were used for in situ mRNA localization as described (McAbee et al., 2005). Tissues were fixed in 2.5% formaldehyde and 0.5% glutaraldehyde and then embedded in paraffin. Ten-micrometer-thick sections were cut, mounted onto slides, and hybridized with digoxigenin-labeled *IRX8* or *IRX9* antisense RNA probe synthesized using the DIG RNA labeling mix (Roche). The hybridization signals were detected with alkaline phosphatase–conjugated antibodies against digoxigenin and subsequent color development with alkaline phosphatase substrates.

Subcellular Localization of Fluorescent Protein–Tagged Proteins

The full-length *IRX8* and *IRX9* cDNAs were amplified by PCR using a high-fidelity DNA polymerase and fused in-frame with GFP cDNA (ABRC). The IRX8-GFP and IRX9-GFP fusion cDNAs were cloned downstream of the cauliflower mosaic virus 35S promoter in the binary vector pBI121. The constructs were transformed into wild-type *Arabidopsis* for the generation of transgenic plants. The GFP signals from roots of 3-d-old transgenic seedlings were observed using a Leica TCs SP2 spectral confocal microscope (Leica Microsystems). Images were processed with Adobe Photoshop version 7.0 (Adobe Systems).

The colocalization of fluorescent protein–tagged IRX8 and IRX9 with a Golgi marker was performed in carrot (*Daucus carota*) protoplasts as described (Zhong et al., 2005). The IRX8 and IRX9 cDNAs were fused in-frame with YFP cDNA and ligated between the cauliflower mosaic virus 35S promoter and the nopaline synthase terminator in a high-copy vector. The IRX8-YFP or IRX9-YFP construct together with the MUR4-CFP construct (Burget et al., 2003) were cotransfected into carrot protoplasts. After 20 h of incubation, the transfected protoplasts were examined for yellow and cyan fluorescent signals using a Leica TCs SP2 spectral confocal microscope.

Immunolocalization of Xylan in the Cell Walls of *Arabidopsis* Stems

Basal internodes of stems from 10-week-old plants were fixed at 4°C overnight with 2% glutaraldehyde in PBS (33 mM Na_2HPO_4, 1.8 mM NaH_2PO_4, and 140 mM NaCl, pH 7.2). After fixation, tissues were dehydrated through a gradient of ethanol and embedded in LR White resin (Electron Microscopy Sciences). One-micrometer-thick sections were cut with a microtome and incubated with the LM10 or LM11 monoclonal antibody, which recognizes GX (Plantprobes) (McCartney et al., 2005), and then with fluorescein isothiocyanate–conjugated secondary antibodies. The fluorescence-labeled sections were observed using a Leica TCs SP2 spectral confocal microscope. Images from single optical sections were collected and processed with Adobe Photoshop. For transmission electron microscopy, 85-nm-thick sections were incubated with the LM10 monoclonal antibody and then with gold (10 nm)-conjugated secondary antibodies. The immunogold-labeled sections were visualized with a Zeiss EM 902A transmission electron microscope (Carl Zeiss).

Breaking Force Measurements

The basal parts of the main inflorescences of 10-week-old *Arabidopsis* plants were measured for their breaking force using a digital force/length tester (model DHT4-50; Larson System). Individual plants of wild type, *irx8-1*, *irx9-2*, and complemented *irx8-1* and *irx9-2* were used for breaking force measurements. The breaking force (*g*) was calculated as the force needed to break apart a stem segment (Zhong et al., 1997).

Histology of *Arabidopsis* Stems

Basal internodes of the inflorescence stems of 10-week-old plants were fixed at 4°C overnight with 2% glutaraldehyde in PBS (33 mM Na_2HPO_4, 1.8 mM NaH_2PO_4, and 140 mM NaCl, pH 7.2). After fixation, tissues were postfixed in 1% (v/v) OsO_4 and then dehydrated through a gradient of ethanol and embedded in Spurr's resin (Electron Microscopy Sciences). One-micrometer-thick sections were stained with toluidine blue for light microscopy. For transmission electron microscopy, 85-nm-thick sections were stained with uranyl acetate and lead citrate and visualized using a Zeiss EM 902A transmission electron microscope.

Isolation and Extraction of Cell Walls

Cell walls were prepared as alcohol-insoluble residues (AIRs) from inflorescence stems from ~200 wild-type or mutant plants. Similar yields of AIRs (80 to 100 mg AIRs/g fresh weight of stems) were obtained for wild-type and mutant plants. Polysaccharides were solubilized (Zhong et al., 2005) by sequential extraction of the AIRs with (1) endopolygalacturonase (10 units; prepared from *Aspergillus niger*) and pectin methylesterase (10 units; prepared from *Aspergillus aryzae*; Novozymes); (2) a xyloglucan-specific endoglucanase (XEG; 7.8 units; Novozymes) purified as described (Pauly et al., 1999); (3) 1 N KOH containing 1% (w/v) $NaBH_4$; and (4) 4 N KOH containing 1% (w/v) $NaBH_4$. The 1 and 4 N KOH extracts were neutralized with glacial acetic acid and then dialyzed against water. After dialysis, >80% of the material remained soluble. GXs with a reducing residue at one end were solubilized by treating *irx9* AIRs (previously extracted with pectin methylesterase/endopolygalacturonase and XEG) with 0.25 N KOH in the absence of $NaBH_4$. A low concentration of KOH was used to minimize base-catalyzed degradation of the reducing end of the polysaccharide (Johansson and Samuelson, 1977). GX in the 0.25 N KOH extract was precipitated by the addition of ethanol (to 80%) containing acetic acid. The precipitated GX was dialyzed and lyophilized.

Glycosyl Residue Composition Analysis

The 1 and 4 N KOH–soluble polysaccharides were converted to alditol acetate derivatives as described (Carpita and Shea, 1989). The derivatives were analyzed by gas chromatography–electron-impact mass spectrometry.

Enzyme Treatment of Cell Wall Extracts and Generation of Xylan Oligosaccharides

The 1 and 4 N KOH–soluble materials were treated for 24 h at 37°C with *Trichoderma viride* endoxylanase (0.04 units/10 mg fraction; Megazyme). The endoxylanase digestion products were separated into neutral and acidic fractions by SEC using a Sephadex G-25 column (90 × 2.5 cm)

eluted with water. Because of their larger size and ionic nature, acidic oligosaccharides were eluted from this matrix before the neutral oligosaccharides. Fractions containing the acidic oligosaccharides were pooled and analyzed by MALDI-TOF MS.

Size-Exclusion Chromatographic Analyses of Xylans

The materials solubilized by treating *Arabidopsis* cell walls with 1 and 4 N KOH were treated separately with endoxylanase. The reaction mixtures were then separated by SEC using a Superose 6 HR10/30 column. The molecular weight distribution of the GX in these alkali extracts was evaluated by comparing the SEC profiles of untreated and endoxylanase-treated materials (see Supplemental Figure 1 online). Polymeric GX was identified in these profiles by its susceptibility to endoxylanase and resistance to XEG treatment (0.78 units/10 mg; Novozymes) (Pauly et al., 1999).

Calculation of the Molecular Properties of the Xylans

The cross-peaks in the COSY NMR spectra were integrated to determine the relative abundances of the tetraglycosyl-xylitol (sequence **2**; Figure 1), the xylosyl-xylitol, and all residues in the reducing oligosaccharides in samples prepared by endoxylanase treatment of KOH-solubilized materials. This enables the average number of residues in the polymer (DP) and the ratio of tetraglycosyl-xylitol to xylosyl-xylitol to be calculated. This gives the percentage of GXs with glycosyl sequence **2** at the end and allows the average molecular weight of the GXs to be calculated, which, in turn, allows the amounts of GX (mg/g AIRs) to be converted to a molar value (μmol/g AIRs).

MALDI-TOF MS

Positive-ion MALDI-TOF mass spectra were recorded using an Applied Biosystems Voyager-DE biospectrometry workstation. Aqueous samples (1 μL of a 1-mg/mL solution) were mixed with an equal volume of matrix solution (0.1 M 2,5-dihydroxbenzoic acid and 0.03 M 1-hydroxyisoquinoline in aqueous 50% MeCN) and dried on the MALDI target plate. Typically, spectra from 200 laser shots were summed to generate a mass spectrum.

^{1}H-NMR Spectroscopy

GX and xylo-oligosaccharides (4 to 8 mg) were dissolved in D_2O (0.7 mL, 99.9%; Cambridge Isotope Laboratories). ^{1}H-NMR spectra were recorded with a Varian Inova NMR spectrometer operating at 600 MHz and with a sample temperature of 298 K. All two-dimensional spectra were recorded using standard Varian pulse programs. Chemical shifts were measured relative to internal acetone (δ 2.225). Resonances were assigned to specific glycosyl residues on the basis of their scalar coupling patterns and chemical shifts. Intraglycosidic scalar couplings and long-range (interglycosidic) scalar couplings were simultaneously detected in gCOSY spectra of the oligosaccharides recorded at high resolution (Jia et al., 2005). Interglycosidic dipolar couplings for oligosaccharides were observed in NOESY spectra recorded using a mixing time of 200 ms. ROESY spectra were recorded with a mixing time of 200 ms and a spin-lock field (γB_1) of 1488 Hz.

Isolation of β-D-Xyl*p*-(1→4)-β-D-Xyl*p*-(1→3)-α-L-Rha*p*-(1→2)-α-D-Gal*p*A-(1→4)-D-Xylitol

Endoxylanase-generated GX oligosaccharides were reacted for 2 h at 65°C and pH 5.5 with 0.2 M 2-aminobenzamide in the presence of 1 M $NaBH_3CN$ to quantitatively convert the reducing oligosaccharides to their fluorescent derivatives (Ishii et al., 2002). The β-D-Xyl*p*-(1→4)-β-D-Xyl*p*-(1→3)-α-L-Rha*p*-(1→2)-α-D-Gal*p*A-(1→4)-D-xylitol was readily separated from the relatively nonpolar 2-aminobenzamide–derivatived xylo-oligosaccharides by reverse-phase HPLC on an octadecyl silica column (Zorbax; RP-18; 25 × 10 cm). Oligosaccharides were eluted with aqueous methanol (0 to 25% [v/v] at 1 mL/min) and detected using a Sedex 55 evaporative light scattering detector (Sedere).

Accession Numbers

Sequence data from this article can be found in the GenBank/EMBL data libraries under the following accession numbers: FRA8 (DQ182567), IRX8 (NM_124850), and IRX9 (NM_129265).

Supplemental Data

The following material is available in the online version of this article.

Supplemental Figure 1. SEC on Superose 6 HR10/30 of the Materials Solubilized by Treating *Arabidopsis* Cell Walls with 1 and 4 N KOH before and after Treatment with Endoxylanase.

ACKNOWLEDGMENTS

This work was supported by grants from the U.S. Department of Energy Bioscience Division (Grant DE-FG02-03ER15415 to Z.-H.Y. and Grants DE-FG05-93ER20097 and DE-FG02-96ER20220 to M.J.P., A.G.D., M.A.O., and W.S.Y.). We thank Carl Bergmann of the Complex Carbohydrate Research Center for the gift of the *A. niger* endopolygalacturonase.

Received December 1, 2006; revised January 22, 2007; accepted February 5, 2007; published February 23, 2007.

REFERENCES

Andersson, S.-I., Samuelson, O., Ishihara, M., and Shimizu, K. (1983). Structure of the reducing end-groups in spruce xylan. Carbohydr. Res. **111:** 283–288.

Aspeborg, H., et al. (2005). Carbohydrate-active enzymes involved in the secondary cell wall biogenesis in hybrid aspen. Plant Physiol. **137:** 983–997.

Bauer, S., Vasu, P., Persson, S., Mort, A.J., and Somerville, C.R. (2006). Development and application of a suite of polysaccharide-degrading enzymes for analyzing plant cell walls. Proc. Natl. Acad. Sci. USA **103:** 11417–11422.

Baydoun, E.A.-H., and Brett, C.T. (1997). Distribution of xylosyltransferases and glucuronyltransferase within the Golgi apparatus in etiolated pea (*Pisum sativum* L) epicotyls. J. Exp. Bot. **48:** 1209–1214.

Baydoun, E.A.-H., Waldron, K.W., and Brett, C.T. (1989). The interaction of xylosyltransferase and glucuronyltransferase involved in glucuronoxylan synthesis in pea (*Pisum sativum*) epicotyls. Biochem. J. **257:** 853–858.

Bechtold, N., and Bouchez, D. (1994). In planta *Agrobacterium*-mediated transformation of adult *Arabidopsis thaliana* plants by vacuum infiltration. In Gene Transfer to Plants, I. Potrykus and G. Spangenberg, eds (Berlin: Springer-Verlag), pp. 19–23.

Becker, D., Kemper, E., Schell, J., and Masterson, R. (1992). New plant binary vectors with selectable markers located proximal to the left T-DNA border. Plant Mol. Biol. **20:** 1195–1197.

Bodevin-Authelet, S., Kushe-Gullberg, M., Pummill, P.E., DeAngelis, P.L., and Lindahl, U. (2005). Biosynthesis of hyaluronan. Direction of chain elongation. J. Biol. Chem. **280:** 8813–8818.

Boerjan, W., Ralph, J., and Baucher, M. (2003). Lignin biosynthesis. Annu. Rev. Plant Biol. **54:** 519–546.

Bouton, S., Leboeuf, E., Mouille, G., Leydecker, M.-T., Talbotec, J., Grainier, F., Lahaye, M., Höfte, H., and Truong, H.-N. (2002). *QUASIMODO1* encodes a putative membrane-bound glycosyltransferase required for normal pectin synthesis and cell adhesion in Arabidopsis. Plant Cell **14:** 2577–2590.

Brown, D.M., Zeef, L.A.H., Ellis, J., Goodacre, R., and Turner, S.R. (2005). Identification of novel genes in *Arabidopsis* involved in secondary cell wall formation using expression profiling and reverse genetics. Plant Cell **17:** 2281–2295.

Burget, E.G., Verma, R., Molhoj, M., and Reiter, W.-D. (2003). The biosynthesis of L-arabinose in plants: Molecular cloning and characterization of a Golgi-localized UDP-D-xylose 4-epimerase encoded by the *MUR4* gene of Arabidopsis. Plant Cell **15:** 523–531.

Carpita, N.C., and Shea, E.M. (1989). Linkage structure of carbohydrates by gas chromatography-mass spectrometry (GC-MS) of partially methylated alditol acetates. In Analysis of Carbohydrates by GLC and MS, C.J. Biermann and G.D. MacGinnis, eds (Boca Raton, FL: CRC Press), pp. 157–216.

Coutinho, P.M., Deleury, E., Davies, G.J., and Henrissat, B. (2003). An evolving hierarchical family classification for glycosyltransferases. J. Mol. Biol. **328:** 307–317.

Crosthwaite, S.K., MacDonald, F.M., Baydoun, E.A.-H., and Brett, C.T. (1994). Properties of a protein-linked glucuronoxylan formed in the plant Golgi apparatus. J. Exp. Bot. **45:** 471–475.

Dalessandro, G., and Northcote, D.H. (1981a). Xylan synthetase activity in differentiated xylem cells of sycamore trees (*Acer pseudoplatanus*). Planta **151:** 53–60.

Dalessandro, G., and Northcote, D.H. (1981b). Increase of xylan synthetase activity during xylem differentiation of the vascular cambium of sycamore and poplar trees. Planta **151:** 61–67.

Ebringerová, A., and Heinze, T. (2000). Xylan and xylan derivatives—Biopolymers with valuable properties. I. Naturally occurring xylans structures, isolation procedures and properties. Macromol. Rapid Commun. **21:** 542–556.

Gregory, A.C.E., Smith, C., Kerry, M.E., Wheatley, E.R., and Bolwell, G.P. (2002). Comparative subcellular immunolocation of polypeptides associated with xylan and callose synthases in French bean (*Phaseolus vulgaris*) during secondary wall formation. Phytochemistry **59:** 249–259.

Ishii, T., Ichita, J., Matsue, H., Ono, H., and Maeda, I. (2002). Fluorescent labeling of pectic oligosaccharides with 2-aminobenzamide and enzyme assay for pectin. Carbohydr. Res. **337:** 1023–1032.

Jia, Z., Cash, M., Darvill, A.G., and York, W.S. (2005). NMR characterization of endogenously *O*-acetylated oligosaccharides isolated from tomato (*Lycopersicon esculentum*) xyloglucan. Carbohydr. Res. **340:** 1818–1825.

Johansson, M.H., and Samuelson, O. (1977). Reducing end groups in birch xylan and their alkaline degradation. Wood Sci. Technol. **11:** 251–263.

Kauss, H., and Hassid, W.Z. (1967). Biosynthesis of the 4-*O*-methyl-D-glucuronic acid unit of hemicellulose B by transmethylation from S-adenosyl-L-methionine. J. Biol. Chem. **242:** 1680–1684.

Kuroyama, H., and Tsumuraya, Y. (2001). A xylosyltransferase that synthesizes β-(1→4)-xylans in wheat (*Triticum aestivum* L.) seedlings. Planta **213:** 231–240.

Lao, N.T., Long, D., Kiang, S., Coupland, G., Shoue, D.A., Carpita, N.C., and Kavanagh, T.A. (2003). Mutation of a family 8 glycosyltransferase gene alters cell wall carbohydrate composition and causes a humidity-sensitive semi-sterile dwarf phenotype in Arabidopsis. Plant Mol. Biol. **53:** 687–701.

Lerouxel, O., Cavalier, D.M., Liepman, A.H., and Keegstra, K. (2006). Biosynthesis of plant cell wall polysaccharides—A complex process. Curr. Opin. Plant Biol. **9:** 621–630.

McAbee, J.M., Kuzoff, R.K., and Gasser, C.S. (2005). Mechanisms of derived unitegmy among Impatiens species. Plant Cell **17:** 1674–1684.

McCartney, L., Marcus, S.E., and Knox, J.P. (2005). Monoclonal antibodies to plant cell wall xylans and arabinoxylans. J. Histochem. Cytochem. **53:** 543–546.

Mukerjea, R., and Robyt, J.F. (2005). Starch biosynthesis: The primer nonreducing-end mechanism versus the nonprimer reducing-end two-site insertion mechanism. Carbohydr. Res. **340:** 245–255.

Orfila, C., Sorensen, S.O., Harholt, J., Geshi, N., Crombie, H., Truong, H.-N., Reid, J.S.G., Knox, J.P., and Scheller, H.V. (2005). *QUASIMODO1* is expressed in vascular tissue of *Arabidopsis thaliana* inflorescence stems, and affects homogalacturonan and xylan biosynthesis. Planta **222:** 613–622.

Pauly, M., Andersen, L.N., Kauppinen, S., Kofod, L.V., York, W.S., Albersheim, P., and Darvill, A.G. (1999). A xyloglucan-specific *endo*-β-1,4-glucanase from *Aspergillus aculeatus*: Expression cloning in yeast, purification and characterization of the recombinant enzyme. Glycobiology **9:** 93–100.

Persson, S., Wei, H., Miline, J., Page, G.P., and Somerville, C.R. (2005). Identification of genes required for cellulose synthesis by repression analysis of public microarray data sets. Proc. Natl. Acad. Sci. USA **102:** 8633–8638.

Porchia, A.C., and Scheller, H.V. (2000). Arabinoxylan biosynthesis: Identification and partial characterization of β-1,4-xylosyltransferase from wheat. Physiol. Plant. **110:** 350–356.

Prydz, K., and Dalen, K.T. (2000). Synthesis and sorting of proteoglycans. J. Cell Sci. **113:** 193–205.

Sakaguchi, H., Watanabe, M., Ueoka, C., Sugiyama, E., Taketomi, T., Yamada, S., and Sugahara, K. (2001). Isolation of reducing oligosaccharide chains from the chondroitin/dermatan sulfate-protein linkage region and preparation of analytical probes by fluorescent labeling with 2-aminobenzamide. J. Biochem. (Tokyo) **129:** 107–118.

Scheible, W.-R., and Pauly, M. (2004). Glycosyltransferases and cell wall biosynthesis: Novel players and insights. Curr. Opin. Plant Biol. **7:** 285–295.

Schmid, M., Davison, T.S., Henz, S.R., Pape, U.J., Demar, M., Vingron, M., Schölkopf, B., Weigel, D., and Lohmann, J. (2005). A gene expression map of Arabidopsis development. Nat. Genet. **37:** 501–506.

Shimizu, K., Ishihara, M., and Ishihara, T. (1976). Hemicellulases of brown rotting fungus, *Tyromyces palustris.* II. The oligosaccharides from the hydrolysate of a hardwood xylan by the intracellular xylanase. Mokuzai Gakkaishi **22:** 618–625.

Somerville, C.R. (2006). Cellulose synthesis in higher plants. Annu. Rev. Cell Dev. Biol. **22:** 53–78.

Sterling, J.D., Atmodjo, M.A., Inwood, S.E., Kumar Kolli, V.S., Quigley, H.F., Hahn, M.G., and Mohnen, D. (2006). Functional identification of an *Arabidopsis* pectin biosynthetic homogalacturonan galacturonosyltransferase. Proc. Natl. Acad. Sci. USA **103:** 5236–5241.

Sugahara, K., and Kitagawa, H. (2002). Heparan and heparan sulfate biosynthesis. IUBMB Life **54:** 163–172.

Suzuki, K., Ingold, E., Sugiyama, M., and Komamine, A. (1991). Xylan synthase activity in isolated mesophyll cells of *Zinnia elegans* during differentiation to tracheary elements. Plant Cell Physiol. **32:** 303–306.

Tlapak-Simmons, V.L., Barron, C.A., Gotschall, R., Haque, D., Cranfield, W.M., and Weigel, P.H. (2005). Hyaluronan biosynthesis by class I streptococcal hyaluronan synthases occurs at the reducing end. J. Biol. Chem. **280:** 13012–13018.

Waldron, K.W., and Brett, C.T. (1983). A glucuronyltransferase involved in glucuronoxylan synthesis in pea (*Pisum sativum*) epicotyls. Biochem. J. **213:** 115–122.

Watt, G., Leoff, C., Harper, A.D., and Bar-Peled, M. (2004). A bifunctional 3,5-epimerase/4-keto reductase for nucleotide-rhamnose synthesis in Arabidopsis. Plant Physiol. **134:** 1337–1346.

Wu, Y.-T., and Liu, J.-Y. (2005). Molecular cloning and characterization of a cotton glucuronosyltransferase gene. J. Plant Physiol. **162:** 573–582.

Ye, Z.-H., York, W.S., and Darvill, A.G. (2006). Important new players in secondary wall synthesis. Trends Plant Sci. **11:** 162–164.

Zhong, R., Burk, D.H., and Ye, Z.-H. (2001). Fibers. A model for studying cell differentiation, cell elongation, and cell wall biosynthesis. Plant Physiol. **126:** 477–479.

Zhong, R., Demura, T., and Ye, Z.-H. (2006). SND1, a NAC domain transcription factor, is a key regulator of secondary wall synthesis in fibers of *Arabidopsis.* Plant Cell **18:** 3158–3170.

Zhong, R., Pena, M.J., Zhou, G.-K., Nairn, C.J., Wood-Jones, A., Richardson, E.A., Morrison, W.H., Darvill, A.G., York, W.S., and Ye, Z.-H. (2005). The *FRA8* gene, which encodes a putative glucuronyltransferase, is essential for normal secondary wall synthesis. Plant Cell **17:** 3390–3408.

Zhong, R., Taylor, J.J., and Ye, Z.-H. (1997). Disruption of interfascicular fiber differentiation in an *Arabidopsis* mutant. Plant Cell **9:** 2159–2170.

Zhou, G.K., Zhong, R., Richardson, E.A., Morrison, W.H., III, Nairn, C.J., Wood-Jones, A., and Ye, Z.-H. (2006). The poplar glycosyltransferase GT47C is functionally conserved with *Arabidopsis fragile fiber8.* Plant Cell Physiol. **47:** 1229–1240.

NOTE ADDED IN PROOF

After acceptance of this manuscript, Persson et al. (2007) published an analysis showing altered secondary wall morphology and reduced xylan and homogalacturonan content in the cell walls of *irx8* plants.

Persson, S., Caffall, K.H., Freshour, G., Hilley, M.T., Bauer, S., Poindexter, P., Hahn, M.G., Mohnen, D., and Somerville, C. (2007). The *Arabidopsis irregular xylem8* mutant is deficient in glucuronoxylan and homogalacturonan, which are essential for secondary cell wall integrity. Plant Cell **19:** 237–255.